ACS OMEGA

http://pubs.acs.org/journal/acsodf

Article

Expression of miR-181a in Circulating Tumor Cells of Ovarian Cancer and Its Clinical Application

Li Zuo, Xiaoli Li, Hailong Zhu, Anqi Li,* and Yonggang Wang*

Cite This: *ACS Omega* 2021, 6, 22011−22019

Read Online

ACCESS | Metrics & More | Article Recommendations

ABSTRACT: *Objective:* To determine the possibility of early diagnosis and prognosis of ovarian cancer (OC) via detecting miR-181a in circulating tumor cells (CTCs) of OC and to solve clinical difficulties in OC tissue sample collection. *Methods:* EpCAM liposome magnetic beads (Ep-LMBs) were prepared by the reverse-phase evaporation method, and the performance of EpCAM was characterized. The cytotoxicity assay was detected by the MTT assay, and CTC capture efficiency was determined using OC cell lines. Blood and tissue samples were collected from 30 patients with OC and 30 normal ovarian tissue samples were selected. Expression of miR-181a in CTCs and tissue samples was measured by real-time fluorescence quantitative PCR (RT-qPCR) with U6 as an internal reference. Expression of miR-181a was interfered in OC cells and its relative expression was measured. *Results:* Ep-LMBs were successfully prepared with high stability. Cellular assays showed that these Ep-LMBs could capture up to 80% of OC cells. RT-qPCR showed that the expression of miR-181a was increased in OC tissues compared with that in normal ovarian tissues, and the relative expressions of miR-181a in cancerous tissues and CTCs were comparable. Correlation analysis with clinical characteristics revealed that miR-181a expression was correlated with the stage and metastasis of OC and the difference was statistically significant. *Conclusion:* MiR-181a may be involved in the development and progression of OC as an oncogene. Detection of miR-181a in Ep-LMB-captured CTCs is an effective and feasible alternative method for early diagnosis and prognostic evaluation of OC other than tissue tests.

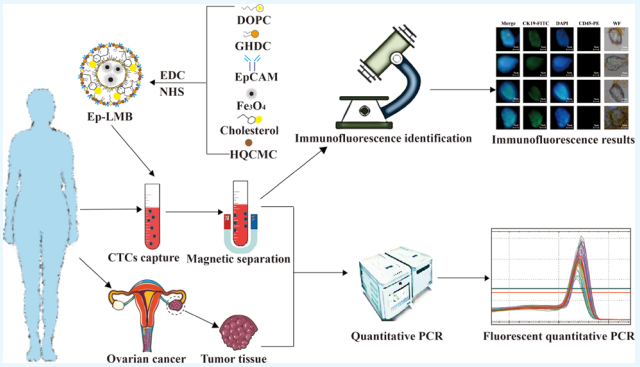

1. INTRODUCTION

Ovarian cancer (OC) is the third largest malignant tumor in the female reproductive system, and its morbidity and mortality remain high. Although surgery combined with traditional chemotherapy has made great progress in the treatment of ovarian cancer, due to the widespread metastasis of ovarian cancer, the vast majority of advanced patients relapse within 5 years.[1,2] Although many biomarkers have been identified as important predictors of ovarian cancer, few can be used as independent predictors. Therefore, the determination of a new biomarker as an independent predictor of the prognosis of ovarian cancer is of great significance for early diagnosis, thereby improving the clinical treatment strategies and prognosis of the disease. Circulating tumor cells (CTCs) refer to the cells that detach from the tumor in situ and enter the blood circulation. These cells have the potential to attach to other parts of the body and form new metastatic foci. The detection of CTCs can be effectively applied to the early diagnosis of tumor in vitro and the monitoring of tumor recurrence.[3,4]

Estrogen receptors (ERs) and progesterone receptors (PRs) are widely distributed in the cells and tissues of female reproductive organs to provide material support for the integrated regulation of estrogen and progesterone. When ER and PR bind to their ligands to form complexes, these complexes are activated and bind to the chromosome at specific sites, which in turn activates genes and initiates the transcription and synthesis of new mRNAs. New proteins with biological functions are then synthesized to regulate cell growth and metabolism.[5] Studies have shown that estradiol may inhibit or activate the expression of miRNAs and regulate the activity of ER via inhibiting the expression of regulatory factors, thereby affecting the metabolism of estradiol or other estrogens. Therefore, abnormally expressed miRNAs may be related to the development of estrogen-related cancers such as breast cancer, endometrial cancer, and OC.[6] MiR-181 is a member of the miRNA family. Studies have shown that miR-181 was overexpressed in rodent hematopoietic progenitor

Received: May 18, 2021
Accepted: August 5, 2021
Published: August 19, 2021

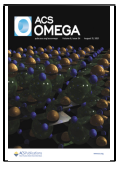

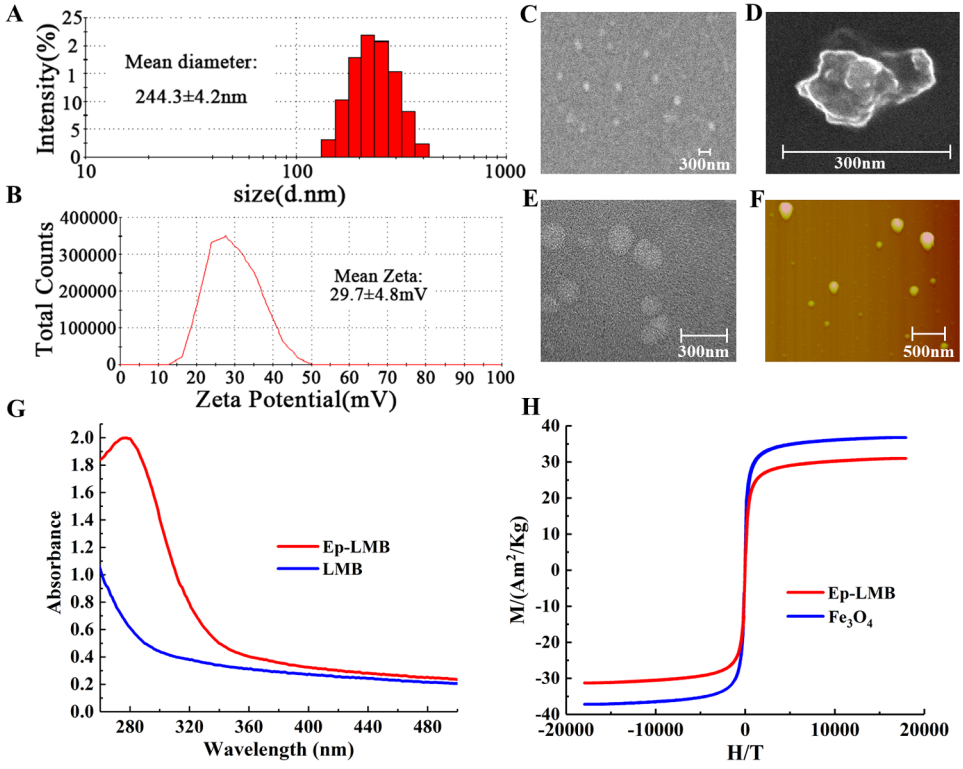

Figure 1. Results of Ep-LMB characterization tests. (A) Particle size distribution; (B) ζ-potential distribution; (C) scanning electron microscopy; (D) scanning electron microscopy; (E) transmission electron microscopy; (F) atomic force observation; (G) UV absorption of LMBs and Ep-LMBs; and (H) the hysteresis curve.

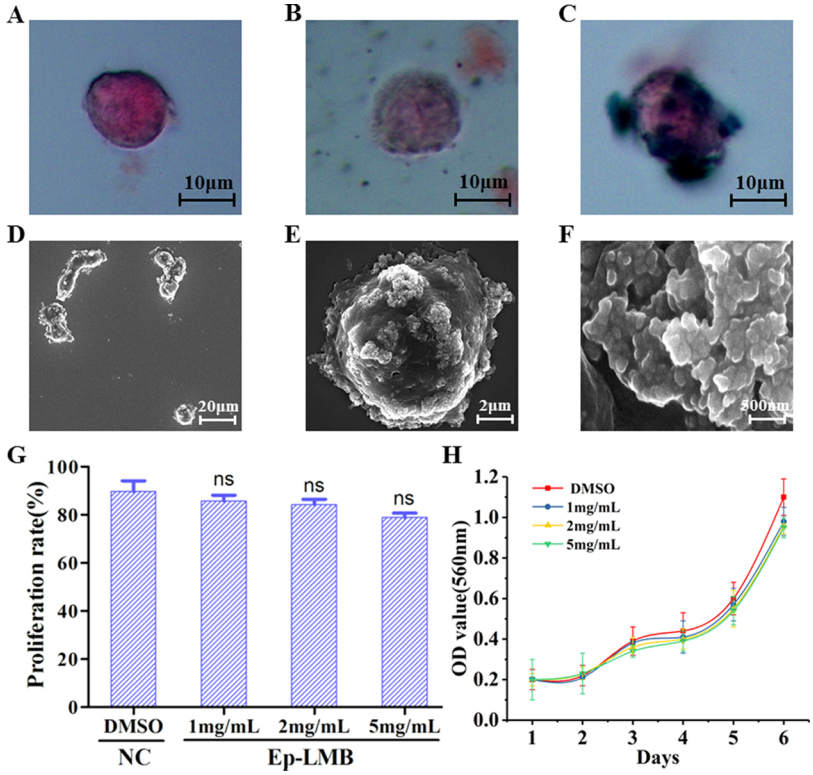

Figure 2. Results of Prussian staining and the results of the cytotoxicity assay. (A) SKOV3 cells; (B) SKOV3 cells captured by LMBs; (C) SKOV3 cells captured by Ep-LMBs; (D) SEM results of ovarian cancer cells captured by Ep-LMBs (2000×); (E) SEM results of ovarian cancer cells captured by Ep-LMBs (20000×); (F) SEM results of ovarian cancer cells captured by Ep-LMBs (200000×); (G) proliferation of SKOV3 cells 72 h after being treated with different concentrations of Ep-LMBs; and (H) growth curve of SKOV3 cells.

https://doi.org/10.1021/acsomega.1c02425
ACS Omega 2021, 6, 22011−22019

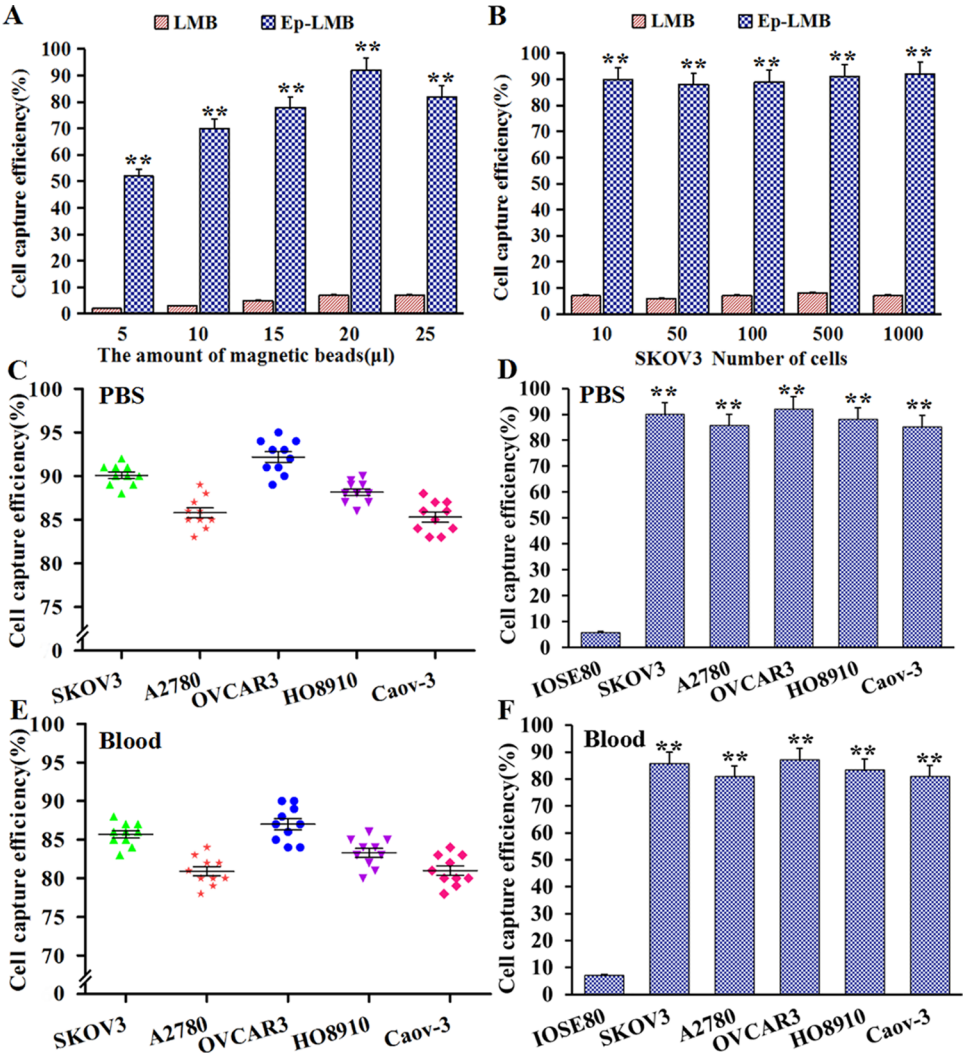

Figure 3. Capture efficiency of Ep-LMB and LMB magnetic spheres on ovarian cancer cells. (A) The capture efficiency of SKOV3 with different magnetic sphere usage; (B) the capture efficiency of SKOV3 cells with different cell gradients; (C) the scatter plot of capture efficiency of Ep-LMBs on different ovarian cancer cell lines in the PBS system; (D) the average capture efficiency of Ep-LMBs on different ovarian cancer cell lines in the PBS system; (E) the scatter plot of capture efficiency of Ep-LMBs to different ovarian cancer cell lines in the blood simulation system; and (F) average capture efficiency of Ep-LMBs on different ovarian cancer cell lines in the blood simulation system.

cells, and the number of B lymphocytes was doubled after the cells were treated under different conditions, while the lymphocytes remained affected, suggesting that miR-181 may play a key role in the development and differentiation of mouse and human cells.[7] MiR-181a regulates the proliferation, development, and differentiation of cells. Abnormal expression of miR-181a is associated with abnormal cell functions and can be detected in various tumors, including leukemia,[8] breast cancer,[9] liver cancer,[10] colorectal cancer,[11] and glioma.[12]

On this basis, the present study was to detect the expression of miR-181a in normal ovary tissues, OC tissues, and liposome magnetic bead (LMB)-captured CTCs from the blood of OC patients by RT-qPCR, to explore the significance of miR-181a in the development and progression of OC, and to analyze the potential involvement of miR-181a in the pathogenesis of OC.

2. RESULTS

2.1. Analysis of Characterization Results. The particle size of Ep-LMBs is shown in Figure 1A. The mean diameter of Ep-LMB particles was 244.3 ± 4.2 nm and the distribution ranged between 147.7 and 412.5 nm. The narrowly distributed particle size indicated the even distribution and favorable stability of Ep-LMB particles. The potential of Ep-LMBs is shown in Figure 1B. The charge of these magnetic beads was 29.7 ± 4.8 mV, and the surface charged microspheres boasted favorable dispersibility due to electrostatic repulsion between each other, which is conducive to the dispersion of microspheres in hydrophilic solution. Moreover, positively charged liposome magnetic beads can easily bind to negatively charged cells. The results of scanning electron microscopy (SEM), transmission electron microscopy (TEM), and atomic force microscopy (AFM) are shown in Figure 1C−F. Ep-LMB magnetic spheres are spherical, with a particle size of about 250 nm, and have regular shapes. They have the characteristics of liposome vesicles and are uniformly distributed without agglomeration. The ultraviolet (UV) analysis demonstrated a broad absorption peak at 280 nm for Ep-LMBs rather than LMBs (Figure 1G). This protein-specific characteristic showed that the EpCAM antibody was attached to the surface of the magnetic beads, ensuring the excellent specificity of these beads. Hysteresis curves of Fe_3O_4 beads and Ep-LMBs are shown in Figure 1H. The saturation magnetizations of Fe_3O_4

https://doi.org/10.1021/acsomega.1c02425
ACS Omega 2021, 6, 22011−22019

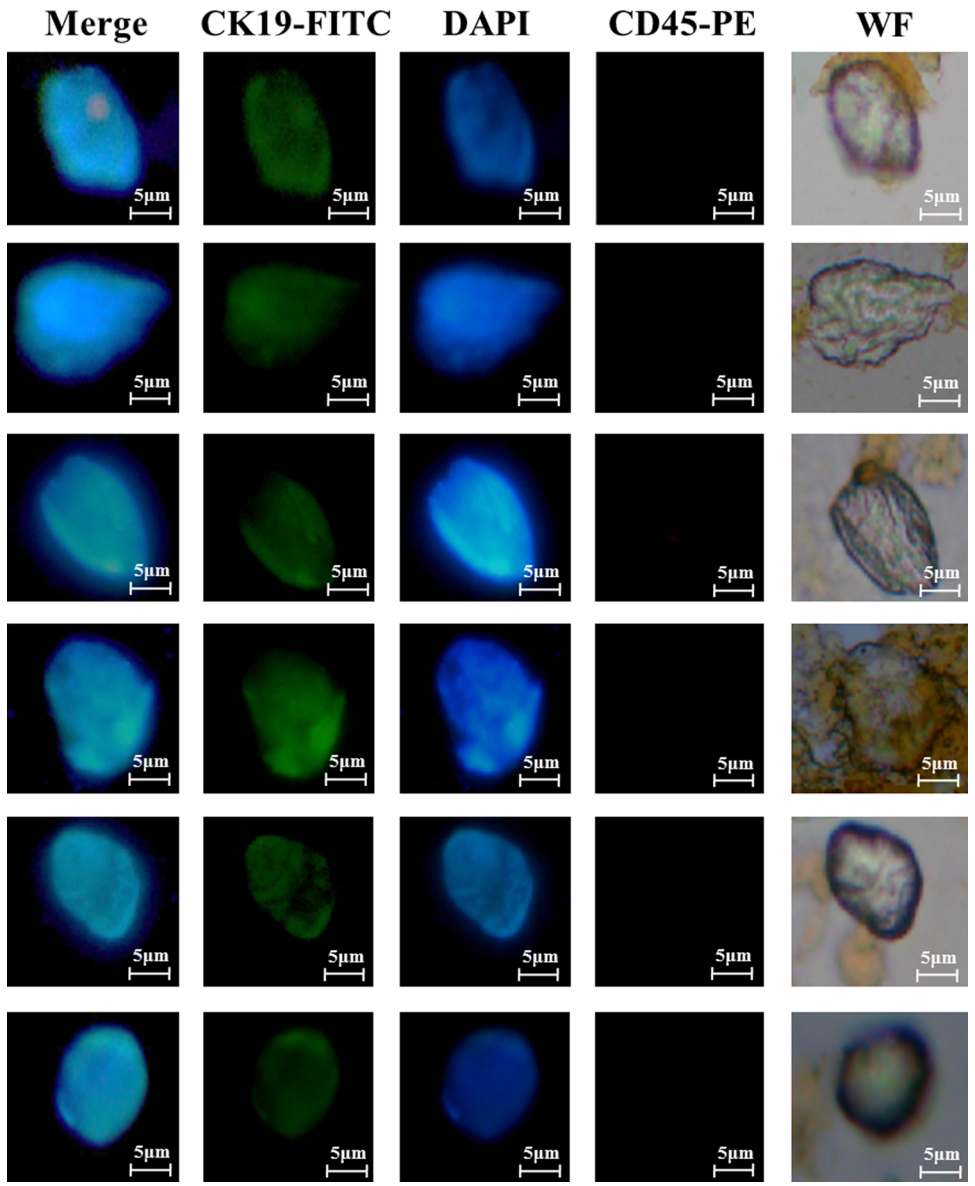

Figure 4. Immunofluorescence identification of OC CTCs captured in blood samples.

and Ep-LMBs were 37.0 and 31.1 Am^2/Kg, respectively. Comparative analysis revealed that the saturation magnetization of Fe_3O_4 decreased slightly after being enwrapped by DOPC and coupled with the EpCAM antibody, indicating that Fe_3O_4 beads were successfully encapsulated by liposomes and connected with the EpCAM antibody. These characterization tests showed that the prepared Ep-LMBs had a small particle size, high stability, favorable dispersibility, and high specificity, which enabled the excellent dispersion of these beads when used for CTC capture.

2.2. Ep-LMB Distribution on the Cell Surface and the Cytotoxicity Assay. The distribution of Ep-LMBs on the surface of SKOV3 cells is shown in Figure 2A−C. Prussian staining of SKOV3 cells showed that SKOV3 cells grew well with a typical and regular shape (Figure 2A). Staining of SKOV3 cells captured by LMBs showed that LMBs were randomly distributed around the cells (Figure 2B) due to the fact that LMBs were nanomagnetic beads with no immune recognition ability to recognize these cells. In Figure 2C, SKOV3 cells were captured by Ep-LMBs and Ep-LMBs were evenly attached to the cell surface, indicating that Ep-LMBs were able to immune recognize SKOV3 cells, which was consistent with the results of the UV test and had no effect on cell morphology. The SEM of Ep-LMBs capturing ovarian cancer cells is shown in Figure 2D−F. Ep-LMBs have been attached to the cell surface. This result is consistent with the results of Prussian blue staining.

Cytotoxicity of Ep-LMBs on SKOV3 cells is shown in Figure 2G,H. The proliferation rates of SKOV3 cells 72 h after being treated with different concentrations of Ep-LMBs were slightly decreased compared with that of the NC group, which was 90.7%, with no significant differences ($P > 0.05$; Figure 2G). It was found in Figure 2H that SKOV3 cells in each Ep-LMB-treated group grew well and no inhibitory effect of Ep-LMBs on cell growth was observed. There was no significant difference in cell growth between each Ep-LMB-treated group and the dimethyl sulfoxide (DMSO) group ($P > 0.05$).We chose 1 mg/mL for subsequent experiments.

2.3. OC Cell Capture Efficiencies of Ep-LMBs and LMBs. The capture efficiency of ovarian cancer cells in

https://doi.org/10.1021/acsomega.1c02425
ACS Omega 2021, 6, 22011−22019

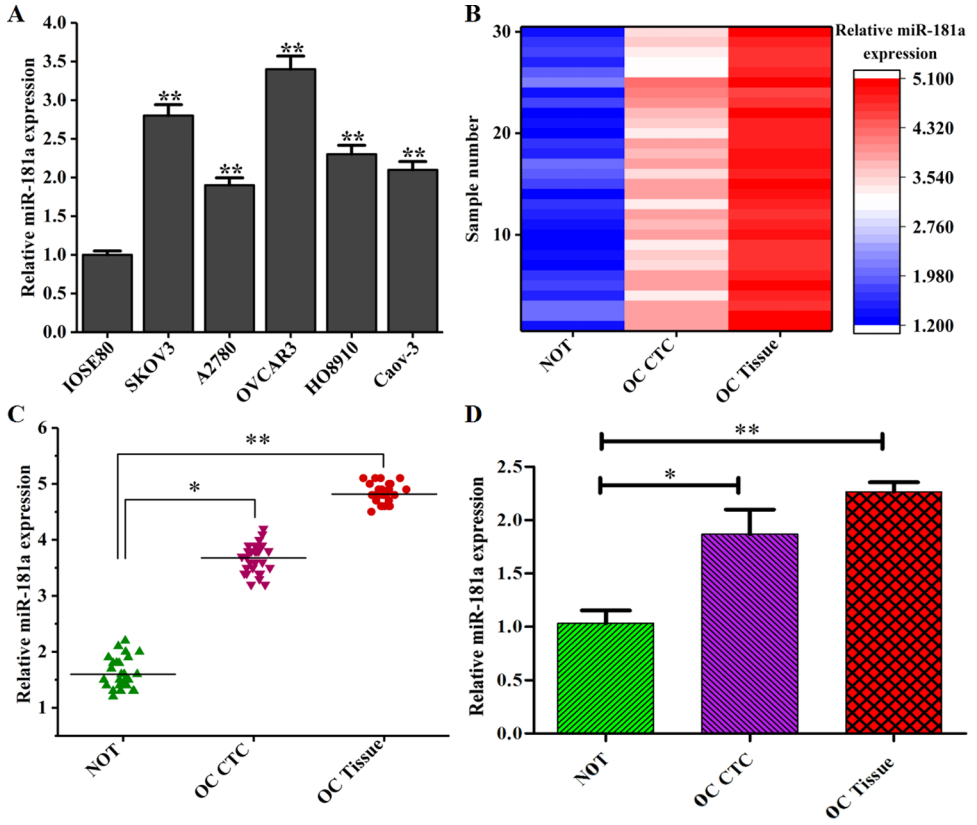

Figure 5. Relative expression of miR-181a in OC CTCs and tissues. (A) The expression of miR-181a in ovarian cancer cell lines and human normal ovarian epithelial cell lines; (B) the expression heat map of miR-181a in ovarian cancer CTCs and tissues; (C) the expression of miR-181a in ovarian cancer CTCs and tissue scatter plot; and (D) miR-181a expression in ovarian cancer CTCs and tissue bar graph (NOT: normal ovarian tissues).

phosphate-buffered saline (PBS) and blood is shown in Figure 3. The capture efficiency of SKOV3 cells in different doses of LMBs and Ep-LMBs is shown in Figure 3A, and the capture efficiency reaches the maximum when the dosage is 20 μL; therefore, we selected 20 μL to carry out gradient experiments on SKOV3 cells and found that the capture efficiency was about 90% in different cell gradients with good sensitivity (Figure 3B). Through the capture verification of different ovarian cancer cell lines in the PBS system, the average capture efficiency was more than 85% and was not specific to normal ovarian epithelial cells (Figure 3C,D). In the blood simulation system, the average capture efficiency was more than 80%, and it was not specific to normal ovarian epithelial cells (Figure 3E,F). Therefore, Ep-LMBs could be used to capture CTCs in clinical samples.

2.4. Identification of CTCs Captured from Blood Samples of Patients with OC. OC CTCs captured by Ep-LMBs were identified by immunofluorescence. A clear cell morphology was observed under a light microscope. CK19-FITC staining showed strong green fluorescence and 4',6-diamidino-2-phenylindole dihydrochloride (DAPI) staining showed strong blue fluorescence, and the two kinds of fluorescence completely overlapped when merged together. CD45 staining was negative to exclude leukocytes. Based on these results, the captured cells were OC CTCs (Figure 4).

2.5. Expression of miR-181a in CTCs and Tissues of OC. RNA concentration and purity were determined by a UV spectrophotometer. The absorbance ratio was between 1.8 and 2.1, indicating that the RNA was intact and pure. After the reverse transcription, quantitative PCR was performed. No undesired peaks were found in the melting curves, indicating that a single amplification product was obtained without any nonspecific amplification. It can be seen from the amplification curves that all of the samples reached the plateau stage, indicating that the reaction conditions were optimal. A linear correlation was found between the value of each reaction tube and the logarithm of the initial copy number of the template, i.e., a smaller value indicated a higher initial copy number and a higher expression of the gene. The relative expression was calculated based on the value obtained from the amplification curves (Figure 5). The expression levels of miR-181 in ovarian cancer cell lines was significantly higher than that in IOSE80 cells ($P < 0.01$; Figure 5A). Therefore, miR-181 may be upregulated in OC. The expression of miR-181a in 30 cases of ovarian cancer tissues and blood CTCs, and 30 cases of normal endometrial tissues. The heat map, scatter map, and bar graph are shown in Figure 5B–D. The expression of miR-181a in OC tissues and CTCs was increased compared with that in normal ovarian tissues, and the relative expression of miR-181a in OC tissues was higher than that in CTCs with a statistically significant difference ($P < 0.05$).

2.6. Correlation between the Expression Level of miR-181a and Other Clinical Features. Correlation analysis of the expression level of miR-181a in OC tissues and CTCs with other clinical features showed that the expression of miR-181a in OC was related to disease stages. The expression level of niR-181a in OC tissues ($P = 0.013$) and CTCs ($P = 0.046$) in patients with stage III + IV OC was significantly higher than that in patients with stage I + II OC, and the difference was statistically significant ($P < 0.05$). In

https://doi.org/10.1021/acsomega.1c02425
ACS Omega 2021, 6, 22011−22019

Table 1. Correlation of the Expression Level of miR-181a in OC Tissues and CTCs with Other Clinical Features ($x + s$)

	OC tissue			CTCs		
clinical features	n	ΔCt	P	n	ΔCt	P
age			0.993			1.052
≥60	11	−2.933 ± 2.199		17	−2.947 ± 2.109	
<60	19	−3.025 ± 2.209		13	−2.899 ± 2.119	
history of diabetes			1.105			0.987
yes	3	−3.288 ± 2.406		5	−3.149 ± 2.525	
no	17	−3.682 ± 2.025		15	−3.801 ± ± 2.525	
FIGO stage			0.013			0.046
stage I+ II	20	−2.926 ± 2.209		15	−3.139 ± 2.415	
stage III + IV	10	−5.156 ± 2.005		15	−5.936 ± 2.215	
histological grade			0.516			0.725
G1	22	−3.149 ± 2.525				
G2+G3	8	−3.801 ± 2.525				
lymphatic metastasis			0.024			0.016
no	25	−3.182 ± 2.369		6	−2.193 ± 2.233	
yes	5	−4.812 ± 2.401		24	−4.926 ± 2.045	
myometrial infiltration			1.033			0.991
≤1/2	27	−3.088 ± 2.406		23	−3.112 ± 2.233	
>1/2	3	−4.682 ± 2.025		7	−3.139 ± 2.125	

addition, the expression of miR-181a in OC tissues and CTCs was also statistically significant related to the presence of lymphatic metastasis ($P < 0.05$). Expression of miR-181a in OC patients with deep myometrial infiltration or poor histological differentiation was higher than that in OC patients with superficial myometrial infiltration or high histological differentiation, and the differences were not statistically significant. No significant association was found between the expression of miR-181a and age and previous history of diabetes ($P > 0.05$) (Table 1).

3. DISCUSSION

Studies have shown that deregulated expression of miR-181a plays an important role in tumorigenesis, including leukemia,[8] breast cancer,[9] liver cancer,[10] colorectal cancer,[11] and glioma.[12] Moreover, miR-18la regulates the expression of B-cell lymphoma/leukemia protein,[13] transforming growth factor-β,[14,15] phosphatase and tensin homologue deleted on chromosome 10, PTEN (PTEN),[15,16] ataxia-telangiectasia mutated (ATM) 16, epithelial growth factor receptor (EGFR),[17] and high mobility group B1 protein to affect the growth and apoptosis of tumor cells. Chen et al.[18] found that the number of B lymphocytes doubled when miR-181 was abnormally overexpressed via retroviral vectors in rodent hematopoietic progenitor cells, while that of T lymphocytes remained stable, suggesting that miR-181 may play a key role in the development and differentiation of mouse and human cells. One miRNA may function as an oncogene and a tumor suppressor gene.[19] As a tumor suppressor gene, miR-181a was downregulated in oral squamous cell carcinoma to inhibit the expression of the target gene K-ras.[20] In osteosarcoma, miR-181a was upregulated to promote the proliferation and invasion of cancer cells and inhibit the apoptosis of these cells as an oncogene.[21]

We compared the expression of miR-181a in the tissues of patients with CTCs and OC. In the present study, the expression of miR-181a was upregulated in OC tissues compared with that in normal ovarian tissues ($P < 0.01$). The expression of miR-181a in CTCs was reduced compared with that in OC tissues with no statistically significant difference ($P > 0.05$) and significantly increased compared with that in normal ovarian tissues ($P < 0.05$). Therefore, we concluded that miR-181a may act as an oncogene and participate in the development and progression of OC. The results also showed that the expression of miR-181a in patients with stage III + IV OC was higher than that in patients with stage I + II OC and the difference was statistically significant, which was related to lymphatic metastasis. The upregulation of miR-181a with the increase of OC stages suggested that miR-181a may play an important role in the progression of OC and serve as an indicator to guide the prognosis evaluation of OC.

A fast and efficient miR-181a detection method is successfully established in the present study. We concluded that miR-181a may act as an oncogene and participate in the development and progression of OC, simultaneously; detection of miR-181a in CTCs versus in tissues showed that miR-181a can be consistently detected in CTCs and tissues, and detection of miR-181a in immunomagnetically captured CTCs is an effective and feasible alternative method other than tissue tests, which effectively solves the clinical difficulties in tissue sample collection and provides favorable references for the studies of other cancers.

4. MATERIALS AND METHODS

4.1. Materials and Instruments. We collected 30 cases of ovarian cancer tissue and blood and 30 cases of normal endometrial tissue from January 2018 to December 2019. The procedures followed in this study were approved by the medical Ethics Committee of our hospital, and samples were collected with the patient signing the relevant informed consent.

The OC cell (SKOV3, A2780, OVCAR3, HO8910, and Caov-3) lines and human normal ovarian epithelial cell (IOSE80) lines were purchased from the Cell Bank of Shanghai Institutes for Biological Sciences, CAS. Dulbecco's modified Eagle's medium (DMEM), fetal bovine serum (FBS), and trypsin were purchased from Gibco, the EpCAM antibody was purchased from Abcam, and PEG-DSPE was purchased from Avanti USA. Fe_3O_4 solution, carboxymethyl chitosan hexadecyl quaternary ammonium salt (HQCMC) CK19-

https://doi.org/10.1021/acsomega.1c02425
ACS Omega 2021, 6, 22011−22019

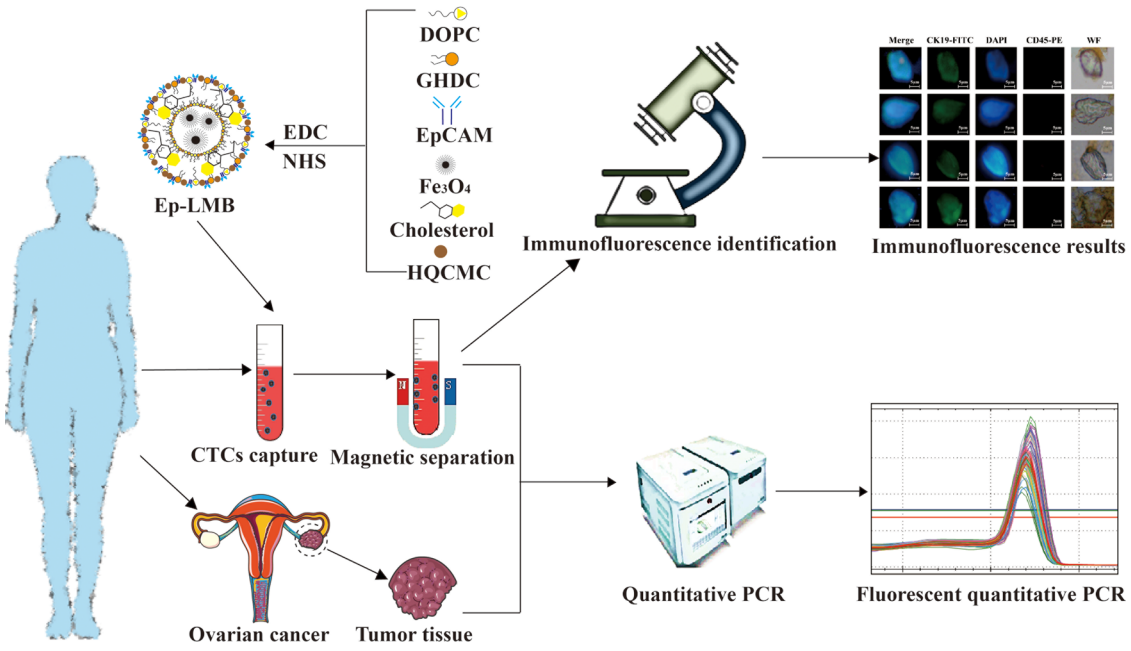

Figure 6. Schematic diagram of the testing process.

FITC, CD45-PE, and DAPI were purchased from Huzhou Lieyuan Medical Laboratory Co., Ltd. 1,2-Dioleoylphosphatidylcholine (DOPC), dimethyl octadecyl epoxypropyl ammonium chloride (GHDC), cholesterol, dichloromethane, *N*-hydroxysuccinimide (NHS), 1-ethyl-3-(3-dimethylaminopropyl)carbodiimide (EDC), and other commonly used reagents were purchased from Sinopharm. TRIzol reagent, reverse transcription kit, and qPCR kit (SYBR Premix Ex Taq II) were purchased from Takara, Lipofectamine 3000 was purchased from Invitrogen, USA, and miR-181a inhibitor was purchased from Ribo Biological, China. A BI-90 Plus laser particle size analyzer/Zeta potentiometer were purchased from Bruker-Haven, An XL-30 environmental scanning electron microscope was purchased from Philips; a Naio atomic force microscope was purchased from Nanosurf, Switzerland; an HT7800 transmission electron microscope was purchased from Hitachi High-Tech, Japan; an Olympus Bx61 fluorescence microscope was purchased from Olympus, Japan; a LightCycler 480II real-time quantitative PCR instrument was purchased from Roche, Switzerland, and a VSM instrument was purchased from Digital Equipment Corporation.

4.2. Preparation of Ep-LMB. Cholesterol, DOPC, DSPE-PEG, GHDC, HQCMC, and Fe_3O_4 solution were dissolved in dichloromethane, and a 0.1 mol/L PBS (pH 7.4) solution was added. A probe ultrasound equipment was used to emulsify the mixture at 25 °C. The power was set at 27% and the duration of ultrasound emulsification was 6 min with 2 min each time followed by 1 min interval. After complete emulsification, the LMB was constructed. The EpCAM antibody (0.6 mg) was dissolved in 10 mL of LMB, and then coupling agents EDC and NHS were added. This mixture was incubated with constant stirring at 4 °C for 24 h and the EpCAM antibody-modified LMB (Ep-LMB) was obtained.[22,23]

4.3. Characterization of Ep-LMB. The Ep-LMB sample (10 μL) was diluted with 1 mL of distilled water and subjected to a BI-90 Plus laser particle size analyzer/Zeta potentiometer. Ep-LMB was observed using an atomic force microscope (AFM). The Ep-LMB sample (10 μL) was diluted with 1 mL of distilled water. Fifty microliters of the mixture was taken and spread on a mica sheet and observed after drying. Ep-LMB was observed using a transmission electron microscope (TEM). A small amount of the freeze-dried Ep-LMB sample powder was taken and dispersed evenly in the aqueous solution by ultrasonic vibration, and then the solution containing the carrier was dropped on the copper mesh with a pipette and kept for 6−8 h to determine its shape and size, followed by making observations. Ep-LMB was observed using a scanning electron microscope (SEM). A small amount of the freeze-dried Ep-LMB sample powder was taken and dispersed ultrasonically with absolute ethanol, and then it was dropped on a copper mesh and kept for 6−8 h to observe its morphology and size. The Ep-LMB sample (10 μL) was diluted with 1 mL of distilled water, and then the absorbance was measured at 280 nm using a UV spectrophotometer. The magnetization intensity of Ep-LMB was measured by the magnetic property measurement system (MPMS).

4.4. Prussian Blue Staining for the Distribution of Ep-LMBs on the Cell Surface. SKOV3 cells were routinely cultured in complete DMEM containing 10% FBS in a humidified incubator at 37 °C, 5% CO_2. The OC cell suspension was prepared and cell density was determined. One hundred cells were added to 7.5 mL of the PBS solution to simulate the CTC suspension. These cells were captured by the prepared LMBs and Ep-LMBs, separately. The captured cells were stained with Prussian blue and observed using a fluorescence microscope. The captured cells were fixed at 4 °C for 1 h, dehydrated by ethanol, dried at room temperature, then dispersed by ultrasonic with absolute ethanol, dropped on a copper net, and observed by a scanning electron microscope.

4.5. Cytotoxicity Assay. The SKOV3 cell suspension was prepared after digestion and cell density was determined with a hemocytometer. One thousand cells were added to each well containing 200 μL of culture medium in a 96-well plate. The cells were treated with Ep-LMBs at concentrations of 1, 2, and 5 mg/mL, separately, and DMSO was used as the normal control (NC) group, with three replicates for each group at

https://doi.org/10.1021/acsomega.1c02425
ACS Omega 2021, 6, 22011−22019

each time point. The cells in the 96-well plate were incubated in a CO_2 incubator for 24 h, and the MTT assay was performed. Briefly, 20 μL of MTT was added to each well and incubated in a CO_2 incubator for 2 h. After the medium was aspirated, 200 μL of DMSO was added to each well and shaken gently using a horizontal shaker for 5 min. The absorbance of each well was measured using a full-wavelength microplate reader at 560 nm. The measurement was continued for 6 days. Data were recorded and analyzed, and growth curves were plotted.

4.6. OC Cell Capture Efficiency of Ep-LMBs. SKOV3, A2780, OVCAR3, HO8910, Caov-3, and IOSE80 cells were routinely cultured in complete DMEM containing 10% FBS in a humidified incubator at 37 °C, 5% CO_2. The OC cell suspension was prepared and cell density was determined. The cells were added to 7.5 mL of the PBS solution and blood to simulate the CTC suspension. These cells were captured by the prepared LMBs and Ep-LMBs, separately. The captured cells were stained with DAPI and observed using a fluorescence microscope. The OC cell capture efficiency of Ep-LMBs was calculated.

4.7. Isolation and Identification of CTCs in Clinical Blood Samples. Twenty microliters of Ep-LMBs were added to 7.5 mL of the blood sample and incubated for 15 min at room temperature (RT) with mixing every 5 min. The centrifuge tube with this mixture was inserted into a magnetic separation rack for 10 min. The blood was discarded, and 10 μL of FITC-labeled CK19 monoclonal antibodies (CK19-FITC), 20 μL of the DAPI staining solution, and 10 μL of the PE-labeled CD45 antibody (CD45-PE) were added after washing with PBS twice. The mixture was mixed and incubated away from light for 15 min. At the end of staining, unbound antibodies and DAPI were washed off with deionized water twice. Magnetic separation was conducted for 5 min. Finally, 15 μL of deionized water was added to the centrifuge tube to resuspend CTCs. The CTC cells obtained are evenly spread on a poly-lysine-coated adhesive slide, dried, and observed under a fluorescence microscope (Figure 6).

4.8. Total RNA Extraction and Quantitative PCR. Total RNA of OC cells, OC tissues, and CTCs captured from the same patient was extracted using the TRIzol reagent kit. Two microliters of the RNA sample was diluted and used to determine the concentration and the OD ratio (OD260/OD280 and OD260/OD230) by a UV spectrophotometer with the absorbance of 0.1% DEPC water as 0; the OD260/OD280 ratio was between 1.8 and 2.1. The OD260/OD230 ratio was more than 1.0, which proved that the extraction effect was good, and the next experiment could be carried out. cDNA was synthesized from the extracted total RNA by reverse transcription according to the instructions of the Takara reverse transcription kit, and qPCR was conducted according to the instructions of the qPCR kit (SYBR Premix Ex Taq II). Primers for miR-181a forward (5′-CTCAACTGGTGTCGTGGAGTCGGCAATTCAGTTGA-GACTCAC-3′), reverse(5′-ACACTCCAGCTGGGAACA TTCAACGCTGTCG-3′) and U6 forward(5′-CTCGCTTCGGCAGCACA-3′), reverse(5′-AACGCTT-CACGAA TTTGCGT-3′) were used. PCR conditions included predenaturation at 95 °C for 6 min, 50 cycles of denaturation at 95 °C for 10 s, annealing at 55 °C for 10 s, and extension at 72 °C for 30 s. At least three experiments were repeated independently and three replicates were set for each sample. The specificity of the product was analyzed according to the melting curves. The relative expression of miRNAs was determined and presented as $\Delta Ct = Ct_{miR\text{-}181a} - Ct_{U6}$, and the fold change of miRNA was calculated as $2^{-\Delta\Delta Ct}$.

4.9. Statistical Analysis. Data were analyzed by SPSS 20.0 statistical analysis software. Comparison between groups was analyzed by the independent sample *t*-test at a significance level of $\alpha = 0.05$. Differences at $P < 0.05$ were statistically significant ($P < 0.05$(*) and $P < 0.01$(**)). All data were presented as the mean value of three independently repeated experiments.

AUTHOR INFORMATION

Corresponding Authors

Anqi Li − *Department of Oncology, Fudan University Shanghai Cancer Center Minhang Branch Hospital, Shanghai 201100, China*; orcid.org/0000-0003-3182-1971; Email: yjs22020@163.com

Yonggang Wang − *Department of Oncology, Affiliated Sixth People's Hospital of Shanghai Jiaotong University, Shanghai 200030, China*; Email: wygzsly@126.com

Authors

Li Zuo − *Department of Oncology, Fudan University Shanghai Cancer Center Minhang Branch Hospital, Shanghai 201100, China*

Xiaoli Li − *Department of Oncology, Fudan University Shanghai Cancer Center Minhang Branch Hospital, Shanghai 201100, China*

Hailong Zhu − *Department of Oncology, Fudan University Shanghai Cancer Center Minhang Branch Hospital, Shanghai 201100, China*

Complete contact information is available at: https://pubs.acs.org/10.1021/acsomega.1c02425

Notes

The authors declare no competing financial interest.

ACKNOWLEDGMENTS

The authors acknowledge the support of the Project of Shanghai Minhang Science and Technology Commission (2017MHZ11) for this work.

REFERENCES

(1) Miranda-Filho, A.; Bray, F.; Charvat, H.; et al. The world cancer patient population (WCPP): An updated standard for international comparisons of population-based survival. *Cancer Epidemiol.* **2020**, *69* (14), 101802−101805.

(2) da Costa, A. A. B. A.; Baiocchi, G. Genomic profiling of platinum-resistant ovarian cancer: The road into druggable targets. *Semin. Cancer Biol.* **2020**, DOI: 10.1016/j.semcancer.2020.10.016.

(3) Kim, M.; Suh, D. H.; Choi, J. Y.; et al. Post-debulking circulating tumor cell as a poor prognostic marker in advanced stage ovarian cancer: A prospective observational study. *Medicine* **2019**, *98* (20), e15354.

(4) Po, J. W.; Roohullah, A.; Lynch, L.; et al. Improved ovarian cancer EMT-CTC isolation by immunomagnetic targeting of epithelial EpCAM and mesenchymal N-cadherin. *J. Circ. Biomarkers* **2018**, *7*, No. 184945441878261.

(5) Klinge, C. M. Estrogen receptor interaction with estrogen response elements. *Nucleic Acids Res.* **2001**, *29*, 2905−2919.

(6) Klinge, C. M. MiRNAs and estrogen action. *Trends Endocrinol. Metab.* **2012**, *23*, 223−233.

(7) Chen, C. Z.; Li, L.; Lodish, H. F.; et al. MicroRNAs modulate hematopoietic lineage differentiation. *Science* **2004**, *303*, 83−86.

(8) Hickey, C. J.; Schwind, S.; Radomska, H. S.; et al. Lenalidomide-mediated enhanced translation of C/EBP-p30 protein up-regulates expression of the antileukemic microRNA-181a in acute myeloid leukemia. *Blood* **2013**, *121*, 159−169.
(9) Bisso, A.; Faleschini, M.; Zampa, F.; et al. Oncogenic miR-181a/b affect the DNA damage response in aggressive breast cancer. *Cell Cycle* **2013**, *12*, 1679−1687.
(10) Brockhausen, J.; Tay, S. S.; Grzelak, C. A.; et al. miR-181a mediates TGF-β-induced hepatocyte EMT and is dysregulated in cirrhosis and hepatocellular cancer. *Liver Int.* **2015**, *35*, 240−253.
(11) Yamashita, S.; Yamamoto, H.; et al. MicroRNA-372 Is Associated with Poor Prognosis in Colorectal Cancer. *Oncology* **2012**, *82*, 205−212.
(12) She, X.; Yu, Z.; Cui, Y.; et al. miR-181 subunits enhance the chemosensitivity oftemozolomide by Rap1 B. -mediated cytoskeleton remodeling in glioblastoma cells. *Med. Oncol.* **2014**, *31*, No. 892.
(13) Zhu, Y.; Wu, J.; Li, S.; et al. The function role of miR-181a in chemosensitivity toadriamycin by targeting Bcl-2 in low -invasive breast cancer cells. *Cell Physiol. Biochem.* **2013**, *32*, 1225−1237.
(14) Brockhausen, J.; Tay, S. S.; Grzelak, C. A.; et al. miR-181a mediates TGF-β-induced hepatocyte EMT and is dysregulated in cirrhosis and hepatocellular cancer. *Liver Int.* **2015**, *35*, 240−253.
(15) Slaby, O.; Lakomy, R.; Fadrus, P.; et al. MicroRNA-181 family predicts response to concomitant chemoradiotherapy with temozolomide in glioblastoma patients. *Neoplasma* **2010**, *57*, 264−269.
(16) Zhang, X.; Deng, H.; et al. MicroRNA-181a Functions as an Oncomir in Gastric Cancer by Targeting the Tumour Suppressor Gene ATM. *Pathol. Oncol. Res.* **2014**, *20*, 381−389.
(17) Pichler, M.; Winter, E.; Ress, A. L.; et al. miR-181a is associated with poor clinical outcome in patients with colorectal cancer treated with EGFR inhibitor. *J. Clin. Pathol.* **2014**, *67*, 198−203.
(18) Chen, C.-Z.; Li, L.; et al. MicroRNAs Modulate Hematopoietic Lineage Differentiation. *Science* **2004**, *303* (5654), 83−86.
(19) Shi, Z.-m.; Wang, X.-f.; et al. MiRNA-181b suppresses IGF-1R and functions as a tumor suppressor gene in gliomas. *RNA* **2013**, *19* (4), 552−560.
(20) Shin, K. H.; Bae, S. D.; Hong, H. S.; et al. miR-181a shows tumor suppressive effect against oral squamous cell carcinoma cells by downregulating K-ras. *Biochem. Biophys. Res. Commun.* **2011**, *404*, 896−902.
(21) Jianwei, Z.; Fan, L.; Xiancheng, L.; et al. Erratum to: MicroRNA 181a improves proliferation and invasion, suppresses apoptosis of osteosarcoma cell. *Tumor Biol.* **2014**, *35*, 11691−11692.
(22) Taylor, M. A.; Sossey-Alaoui, K.; Thompson, C. L.; et al. TGF-β upregulates miR-181a expression to promote breast cancer metastasis. *J. Clin. Invest.* **2012**, *123*, 150−163.
(23) Nishimura, J.; Handa, R.; Yamamoto, H.; et al. microRNA-181a is associated withpoor prognosis of colorectal cancer. *Oncol. Rep.* **2012**, *28*, 2221−2226.

https://doi.org/10.1021/acsomega.1c02425
ACS Omega 2021, 6, 22011−22019